Disorder and phase transitions in $Rb_{1-x}K_xCaF_3$: an electron paramagnetic resonance investigation

1991 J. Phys.: Condens. Matter 3 2535

(http://iopscience.iop.org/0953-8984/3/15/009)

J. Phys.: Condens. Matter 3 (1991) 2535–2544. Printed in the UK

Disorder and phase transitions in $Rb_{1-x}K_xCaF_3$: an electron paramagnetic resonance investigation

J Y Buzaré and P Foucher
Equipe de Physique de l'Etat Condensé, Unité de Recherche Associée au CNRS No 807, Université du Maine, Route de Laval, 72017 Le Mans Cédex, France

Received 11 September 1990, in final form 8 January 1991

Abstract. The electron paramagnetic resonance spectrum of the Gd^{3+}–O^{2-} pair substituted for a Ca–F bond is monitored in order to investigate disorder and phase transitions in mixed fluoperovskites $Rb_{1-x}K_xCaF_3$ for $x = 0.05$ and 0.2. Through computer reconstruction of the spectra, we get detailed information about the disorder around the probe, which shows the substituted K^+ ions to be randomly distributed. At low temperature, two successive structural phase transitions are evidenced and a partial phase diagram is tentatively drawn.

1. Introduction

In fluoperovskite crystals (AMF_3), structural phase transitions (SPT) caused by the condensation of zone boundary modes associated with rotations of MF_6 octahedra have attracted a great deal of interest in the recent past. It has been shown that they may exhibit quite different behaviours.

For instance, $RbCaF_3$ is a cubic crystal at room temperature. It undergoes at $T_{c1} = 195$ K a cubic to tetragonal SPT, which has been extensively investigated by several experimental methods over the past few years: neutron scattering (Rousseau *et al* 1977, Almairac *et al* 1977), x-ray diffraction (Ridou *et al* 1977), electron paramagnetic resonance (Buzaré *et al* 1977, 1980) and nuclear magnetic resonance (Bulou *et al* 1979). This phase transition is weakly first-order and involves the condensation of the R_{25} soft mode. It is followed at $T_{c2} = 50$ K by an order–disorder phase transition giving rise to an orthorhombic phase (Bulou *et al* 1980a, b, Ridou *et al* 1981).

On the other hand, $KCaF_3$ is orthorhombic at room temperature and cubic at high temperature ($T > 560$ K). It shows two transitions at $T_{c1} = 560$ K (Bulou *et al* 1980a, b) or 545 K (Hidaka *et al* 1984) and $T_{c2} = 551$ or 538 K. The former is caused by mode condensation at the M and R points simultaneously and the latter by condensation at the R point.

Together they form mixed crystals, $Rb_{1-x}K_xCaF_3$, over the whole range of concentration, which retain the cubic perovskite structure at high temperature. Owing to the fact that the cation seems to play a fundamental role in stabilizing the structure, one may expect that the substitution of K for Rb changes the interaction and reduces the correlation effects between CaF_6 octahedra. This should result in a randomization of the system. To our knowledge, only a few studies have been achieved on mixed

0953-8984/91/152535 + 10 $03.50

fluoperovskites: $Rb_xK_{1-x}MnF_3$ (Borsa *et al* 1977), $K_xNa_{1-x}MnF_3$ (Ratuszna 1984) and $K_{1-x}Rb_xCdF_3$ (Hidaka *et al* 1990).

Recently, we undertook investigations of the SPT in $Rb_{1-x}K_xCaF_3$ mixed crystals with different experimental techniques (Foucher *et al* 1990). In this paper, we emphasize electron paramagnetic resonance (EPR) results.

Supported by previous successful EPR investigations of SPT in $RbCaF_3$ with the Gd^{3+}–O^{2-} pair substituted for a Ca–F bond as a local probe (Buzaré *et al* 1977, 1980, 1985, 1989, Simon *et al* 1982, Buzaré and Simon 1984), we decided to use this probe in the mixed crystals too. Indeed, because of the O^{2-} substitution for a F^- ion, a strong axial crystal field exists at the Gd^{3+} site whose axis is directed along the Gd^{3+}–O^{2-} pair centre axis. This yields a strong anisotropy of the EPR lines for rotations of the octahedra perpendicular to the pair axis.

2. Experimental details

Single crystals of $Rb_{1-x}K_xCaF_3$ used in these experiments were doped with Gd_2O_3 and grown by the Bridgman–Stockbarger method.

The EPR spectra were recorded on a Bruker X-band spectrometer ($\nu \simeq 9.5$ GHz). The static magnetic field may be varied from 0 to 10 kG. At low temperature, we used a helium gas-flow cryostat (Oxford Instruments). The temperature stability was better than 0.1 K. This temperature corresponds to that of the gas measured at 1 cm from the sample. Depending on the gas flow, it may not differ from that of the sample by more than ± 5 K. In the previous paper (Foucher *et al* 1990), experiments were achieved using the standard Bruker variable-temperature system, where the temperature at the sample is established by regulating the temperature of N_2 gas streaming past the sample, and may be varied in the range 300–100 K only. Some discrepancy appears in the measured temperatures between the two series of experiments, which may be explained by the different variable-temperature systems used.

3. Local order in $Rb_{1-x}K_xCaF_3$ at room temperature

The resolution of the EPR spectra lowers when x increases. Then, the experiments were performed on mixed crystals with low values of x (0.05 and 0.2) for which the resolution of the spectra was satisfactory. In this way, we were able to study the room-temperature cubic phase and get reliable information on the disorder induced by the substituted K^+ ions in the neighbourhood of the paramagnetic probe.

The EPR spectra $RbCaF_3$: Gd^{3+}–O^{2-} have been previously described and interpreted with a spin Hamiltonian $\mathcal{H}_0$ reflecting the tetragonal symmetry of the centre with a large value of the quadrupolar crystal-field parameter b_2^0 (Buzaré *et al* 1977, 1981):

$$\mathcal{H}_0 = g\beta HS + \tfrac{1}{3}b_2^0O_2^0 + \tfrac{1}{60}(b_4^0O_4^0 + b_4^4O_4^4) + \tfrac{1}{1260}(b_6^0O_6^0 + b_6^4O_6^4)$$

where $S = 7/2$. The g-factor was found to be isotropic. The spin Hamiltonian parameters

Table 1. Spin Hamiltonian parameters (in 10^{-4} cm^{-1} except g) of the Gd^{3+}–O^{2-} pair in pure $RbCaF_3$.

g	b_2^0	b_4^0	b_6^0	b_4^4	b_6^4
1.9915	−2590	11	0	−104	−12
±0.0005	±25	±5	±5	±10	±5

are given in table 1 and correspond to the set of axes $OXYZ$ where OZ is along the Gd^{3+}–O^{2-} bond and OX and OY are along the other two fourfold cubic axes. Note that a rotation $\pi/4$ about OZ changes the sign of b_4^4 and b_6^4.

In $Rb_{1-x}K_xCaF_3$, every line observed in pure $RbCaF_3$ is broadened and flanked by satellites (figure 1). The widths of all the observed lines increase with x, as do the relative intensities of the satellites. These additional lines reflect the distribution of the local crystal fields at the Gd^{3+} sites and may be attributed to Gd^{3+}–O^{2-} pairs surrounded by n K^+ ions and $(8-n)$ Rb^+ ions, as next-nearest neighbours ($n = 1, 2, \ldots, 8$).

3.1. Computer simulation of the EPR spectra: basic assumptions

The substitution of K^+ for Rb^+ ions in the $RbCaF_3$ cell lowers the local symmetry at the Gd^{3+} site. Then, the corresponding spin Hamiltonians should take the most general form, which may be written

$$\mathcal{H} = \beta HgS + \sum_n \sum_m (B_n^m O_n^m + A_n^m \Omega_n^m)$$

where n and m are integers: $n = 2, 4$ and 6 and $0 \leqslant m \leqslant n$. Here, we use Al'tschuler and Kozyrev's (1974) notations.

We undertook to determine the spin Hamiltonian parameters corresponding to the different local crystal fields in order to gain a quantitative insight into the disorder induced by the substituted K^+ ions. This work was achieved by computing the EPR spectra by means of some simplifying assumptions. A fine agreement between the computed and experimental spectra would indicate the correctness of the assumptions *a posteriori*. These assumptions are the following:

(i) The K^+ and Rb^+ ions are distributed at random. Then, for a given value of x, the proportion $P_n(x)$ of cells C_n containing n K^+ may be expressed according to

$$P_n(x) = \frac{8!}{n!(8-n)!} x^n (1-x)^{8-n}.$$

(ii) For a cell C_0 ($n = 0$), the Hamiltonian of the Gd–O pair is like the Hamiltonian $\mathcal{H}_0$ of the pair in pure $RbCaF_3$. For a cell C_n ($n > 0$), symmetry lowering results in additional terms in the Hamiltonians previously written $\mathcal{H}$. Among these terms, it is sufficient to retain the quadrupolar terms only, which yields

$$\mathcal{H} = \mathcal{H}_0 + \tfrac{1}{3}(\Delta b_2^0 O_2^0 + b_2^1 O_2^1 + a_2^1 \Omega_2^1 + b_2^2 O_2^2 + a_2^2 \Omega_2^2).$$

The Δb_2^0, b_2^m and a_2^m are supposed to be much smaller than b_2^0 in $\mathcal{H}_0$.

It is worth noting that a cell C_n may correspond to C_8^n possible Gd^{3+} sites. Among these different sites, those which transform into one another by symmetry would have identical spin Hamiltonian parameters if the sets of axes are chosen in a suitable manner.

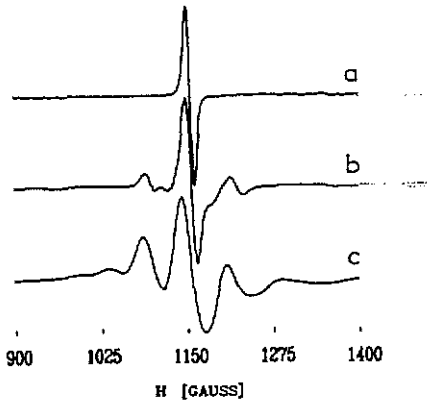

Figure 1. Typical x dependence of an EPR line in $Rb_{1-x}K_xCaF_3:Gd^{3+}$–O^{2-} for $H \| [111]$ and $H_{rf} \| [\bar{1}10]$: (*a*) $x = 0$, (*b*) $x = 0.05$ and (*c*) $x = 0.2$.

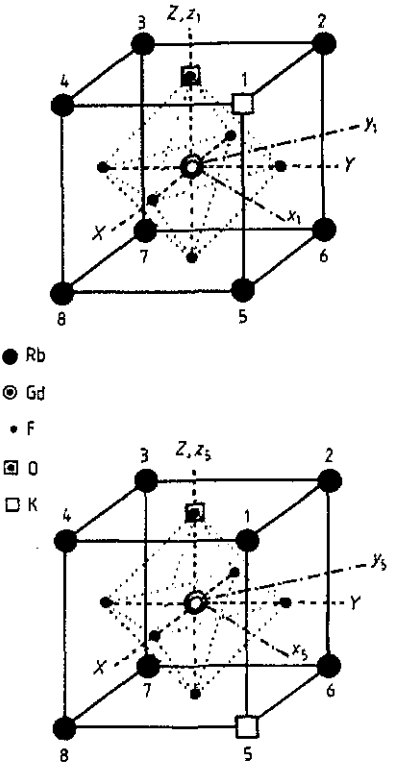

Figure 2. The two types of C_1 cells.

For instance, consider the cells C_1 containing one K^+ ion. In that case, there are eight different sites. However, they may be described by only two sets of spin Hamiltonian parameters connected with the two types of cells in figure 2: the first type corresponds to a K^+ substituted for a Rb^+ ion with a O^{2-} as nearest neighbour (further called $C_{1,O}$ cells); the second one is for a K^+ ion with a F^- as nearest neighbour (called $C_{1,F}$ cells). A further simplification occurs when one expresses the spin Hamiltonian in a set of axes $Ox_iy_iz_i$ with $Oz_i \equiv OZ$ and Ox_i oriented along the direction of the projection of the $Gd^{3+}-K_i^+$ on the XOY plane. Here i stands for one of the eight vertices of the cubic cell (figure 2). Given that x_iOZ is a plane of symmetry in this set of axes, it follows that a_2^1 and a_2^2 are equal to zero. Thus, six parameters are sufficient to take into account the eight C_1 cells. Three of them $\Delta b_{2,O}^0$, $b_{2,O}^1$ and $b_{2,O}^2$ are related to the first type of substitution ($i = 1, 2, 3, 4$); the other three parameters denoted $\Delta b_{2,F}^0$, $b_{2,F}^1$ and $b_{2,F}^2$ are connected with the second one ($i = 5, 6, 7, 8$).

(iii) The last assumption concerns the estimate of the parameters for the cells C_n with $n > 1$. We suppose that the contributions of the substituted K^+ ions as next-nearest neighbours of a Gd^{3+} ion are additive. This allows us to evaluate the spin Hamiltonian parameters in the following manner.

First, we choose a single set of axes in which all the spin Hamiltonians $\mathcal{H}_0$ and $\mathcal{H}$ are expressed. The simplest one is $OXYZ$, previously defined.

Table 2. Spin Hamiltonian parameters (in 10^{-4} cm^{-1}) of the Gd^{3+}–O^{2-} pair in $Rb_{1-x}K_xCaF_3$ for the $C_{1,O}$ and $C_{1,F}$ cells.

$\Delta b^0_{2,O}$	$b^1_{2,O}$	$b^2_{2,O}$	$\Delta b^0_{2,F}$	$b^1_{2,F}$	$b^2_{2,F}$
$+(40 \pm 5)$	$\pm(550 \pm 50)$	$+(10 \pm 2)$	$-(10 \pm 2)$	$\pm(80 \pm 20)$	$-(50 \pm 5)$

Secondly, we calculate the spin Hamiltonian parameters of the C_1 cells in $OXYZ$, which have to be written

$$\Delta b^0_{2,i} = \Delta b^0_{2,L} \qquad b^m_{2,i} = b^m_{2,L}\cos(m\varphi_i) \qquad a^m_{2,i} = b^m_{2,L}\sin(m\varphi_i)$$

where φ_i is the angle (XOx_i) and L stands for O or F according to whether $i = 1$ to 4 or $i = 5$ to 8 respectively.

Thirdly, we calculate the parameters of the cells C_n from the C_1 cell parameters with the following formulae:

$$\Delta b^0_2 = \sum_i \Delta b^0_{2,i} \qquad b^m_2 = \sum_i b^m_{2,i} \qquad a^m_2 = \sum_i a^m_{2,i}.$$

The summation extends over the n K^+ ions in the C_n cell.

3.2. Results and discussion

As may be understood from the preceding paragraph, we need only to determine the two sets of spin Hamiltonians of the C_1 cells in order to be able to reconstruct all the spectra. Indeed, all the parameters for the C_n cells are expressed with $\Delta b^0_{2,L}$, $b^1_{2,L}$ and $b^2_{2,L}$ where L stands for O or F according to the substitution.

These parameters were found by simulating the spectra obtained in $Rb_{0.95}K_{0.05}CaF_3$: Gd^{3+}–O^{2-}. In this crystal, the C_0 and C_1 cells are preponderant and the satellites may be unambiguously attributed to the C_1 cells. A large number of lines were simulated, which correspond to different orientations of the crystal in the magnetic field H, and x was considered as a given parameter equal to the initial K^+ concentration in the melt. All the calculated spectra fitted the experimental ones satisfactorily, as shown in figure 3(*a*).

The two sets of parameters are given in table 2: we were unable to determine the absolute sign of the $\Delta b^1_{2,L}$ from these investigations, but further considerations will allow us to get them (see below). The lineshape is a mixture of Lorentzian and Gaussian. The spectra were simulated with a linewidth $L_0(x)$ for the C_0 cells and two linewidths for the C_1 cells $L_{1,O}(x)$ and $L_{1,F}(x)$: it was impossible to obtain good results if these two linewidths were taken equal. Typical values of these parameters are given in the caption of figure 3.

In figure 3(*b*), the contributions of the C_n ($n = 0, 1, 2$) cells are shown separately. C_2 cells are really negligible as assumed previously. From this reconstruction, it was possible to assign the different lines to the different C_1 cells: the two outer lines are related to the $C_{1,F}$ cells while the inner ones correspond to the $C_{1,O}$.

In order to complete our analysis, we achieved the computer reconstruction of the spectra obtained for the more heavily K-doped compound, i.e. $Rb_{0.8}K_{0.2}CaF_3$. This was done by considering the C_0, C_1 and C_2 cells only. The results were quite satisfactory (figure 4), which prompts us not to take more K^+ substituted cells into account. Note

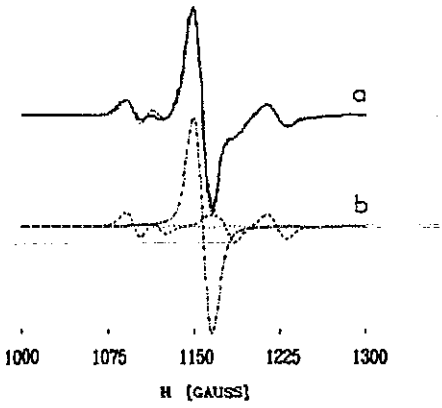

Figure 3. (*a*) Experimental (———) and calculated (– · – · –) spectra in $Rb_{0.95}K_{0.05}CaF_3:Gd^{3+}$–$O^{2-}$ for $H\|[111]$ and $H_{rf}\|[\bar{1}10]$. (*b*) Separate contributions of the C_0 (– · – · –), C_1 (– – – –) and C_2 (. . . .) cells with the following linewidths: $L_0 \simeq L_{1,O} \simeq L_{1,F} \simeq L_2 \simeq 15$ G.

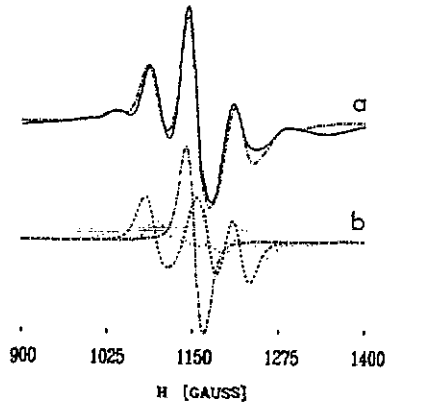

Figure 4. (*a*) Experimental (———) and calculated (– · – · –) spectra in $Rb_{0.8}K_{0.2}CaF_3:Gd^{3+}$–$O^{2-}$ for $H\|[111]$ and $H_{rf}\|[\bar{1}10]$. (*b*) Separate contributions of the C_0 (· – · – ·), C_1 (– – – –) and C_2 (· · · ·) cells with the following linewidths. $L_0 \simeq 26$ G, $L_{1,O} \simeq 30$ G, $L_{1,F} \simeq 28$ G and $L_2 \simeq 34$ G.

the linewidths are approximately twice as large as for $x = 0.05$. This observed line broadening increasing with x is one of the reasons why the contribution of the C_n cells ($n \geqslant 3$) is unimportant in the present case.

These results indicate that the line positions are mainly affected by the next-nearest neighbours of the Gd^{3+}–O^{2-} pair, and substitutions occurring farther from the probe affect the linewidths only: the pair is a short-range probe, which provides us with information about the local order. They show clearly that no chemical order occurs in the mixed compounds that have been investigated ($x \leqslant 0.2$). Furthermore, we can infer the value of x from the reconstruction of the spectra. Similar conclusions were drawn in the case of mixed $Rb_x(NH_4)_{1-x}AlF_4:Fe^{3+}$ (Jouanneaux *et al* 1989).

The determination of the spin Hamiltonian parameters of the Gd^{3+}–O^{2-} in the C_1 cells allows us to estimate the displacements of the ions in such cells. It has been shown by Newman and Urban (1975) that the Gd^{3+} spin Hamiltonian parameters can be constructed from the superposition of single ligand contributions. In accordance with this superposition model, each b_n^m can be expressed as

$$b_n^m = \sum_l \bar{b}_n^{(l)}(R_l) K_n(\theta_l, \varphi_l)$$

where R_l, θ_l and φ_l are the coordinates of the ligand l and K_n^m are real spherical harmonics. The $\bar{b}_n^{(l)}(R_l)$ are functions of the radial metal–ligand distance R_l, which are intrinsic parameters. In pure $RbCaF_3$ ($R_0 = 2.227$ Å), it was found (Buzaré *et al* 1981) that

$$\bar{b}_2^{(O)} = -2060 \times 10^{-4}\ \text{cm}^{-1} \qquad \bar{b}_2^{(F)} = 540 \times 10^{-4}\ \text{cm}^{-1}.$$

Assuming that the most important contribution to the b_2^m parameters is due to the nearest O^{2-} ion, the results of table 2 that correspond to a K^+ ion substituted for a Rb^+ with an O^{2-} as nearest neighbour are compatible with a variation of $\bar{b}_2^{(O)}$ equal to $40 \times 10^{-4}\ \text{cm}^{-1}$, which accounts for a very small variation of the Gd–O distance, and a rotation of this bond $\Delta\theta = \pm 2.5°$ in the Ox_iZ plane. The polarizability of the Rb^+ ion

(1.50 Å^3) being larger than the K^+ one (0.97 Å^3), we may infer that the O^{2-} ion moves towards the Rb^+ and then we retain as the correct solution

$$\Delta\theta = -2.5°$$

which corresponds to

$$b^1_{2,O} = 550 \times 10^{-4}\ \text{cm}^{-1}.$$

From table 2, it is not so easy to obtain definite conclusions about the distortion, when the substituted K^+ has an F^- as nearest neighbour, but it may be seen that the distortion is undoubtedly very small.

4. Evidence for two successive phase transitions in $Rb_{1-x}K_xCaF_3$

As previously outlined, the spectrum of the Gd^{3+}–O^{2-} pair in pure $RbCaF_3$ exhibits strong axial lines corresponding to the large b^0_2 parameter. Details about this EPR spectrum were given by Buzaré *et al* (1977, 1980, 1981) and Simon *et al* (1982).

Most of the previous EPR (X-band) investigations of the cubic to tetragonal phase transition were achieved by monitoring the so-called A lines: two components connected with pairs along [100] and [010] whose effective g-factors vary between $g^{\text{eff}}_{\parallel} \simeq 2$ and $g^{\text{eff}}_{\perp} = 7.324$ and one isotropic component due to pairs along [001] with $g^{\text{eff}} = 7.324$. In the cubic phase when $H \| [110]$, the lines due to pairs pointing along [100] and [010] coincide. In the tetragonal phase ($T < T_{c1}$), octahedral rotations by $\pm\Phi$ around [001] result in a splitting ΔH of these lines proportional to Φ (36 G deg^{-1}), whereas rotations around [100] and [010] induce a far smaller splitting. Furthermore, whichever the rotation is, the isotropic A line remains unaffected.

This interesting feature was used to investigate the phase transitions in the mixed compounds $Rb_{1-x}K_xCaF_3$. Then, we studied the behaviour of these A lines as a function of temperature when H is along [110]. The radio frequency field H_{rf} is along [001]. It may be pointed out that only lines due to pairs in C_0 cells are sufficiently resolved to be unambiguously observed.

4.1. $Rb_{0.95}K_{0.05}CaF_3$

Figure 5 exhibits this dependence for $Rb_{0.95}K_{0.05}CaF_3$ between room temperature and 180 K. The spectrum ($T = 210$ K) in figure 5(*a*) is characteristic of the cubic phase: the single A line ($H \simeq 920$ G) and the double one ($H \simeq 1250$ G) are due to pairs along [001] and [100] or [010] respectively. The double A line broadens strongly on cooling down to 210 K. Figure 5(*b*) ($T = 209$ K) shows the double A line split into three components, while the single one does change. Obviously, a phase transition occurs at $T_{c1} \simeq 210$ K. On cooling further (see spectra in figures 5(*c*) and (*d*) at $T = 207$ and 180 K), the splitting of the two outer components increases while the central one broadens. This behaviour may be related to a cubic to tetragonal phase transition as previously observed in pure $RbCaF_3$: the two outer lines may be attributed to Gd^{3+}–O^{2-} pairs in octahedra rotated about [001] by $\pm\Phi$; the central component is due to pairs in octahedra rotated about [100] or [010]. The splitting between the two outer lines is proportional to the rotational angle Φ of the octahedra: Φ is found to vary between 2° at $T = 209$ K (figure 5(*b*)) and 4° at $T = 180$ K (figure 5(*d*)).

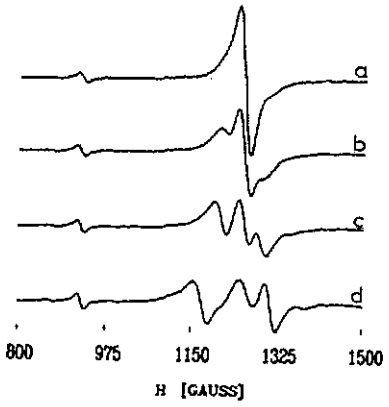

Figure 5. Temperature dependence of the A lines in $Rb_{0.95}K_{0.05}CaF_3$ about the first SPT: (*a*) T = 210 K, (*b*) 209 K, (*c*) 207 K and (*d*) 180 K.

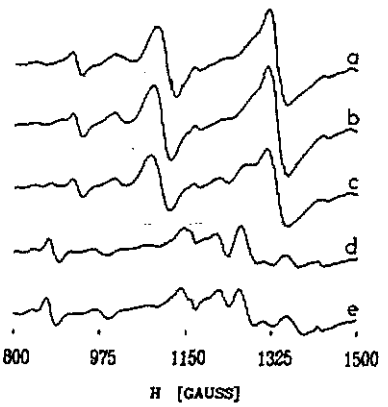

Figure 6. Temperature dependence of the A lines in $Rb_{0.95}K_{0.05}CaF_3$ about the second SPT: (*a*) T = 110 K, (*b*) 90 K, (*c*) 80 K, (*d*) 79 K and (*e*) 60 K.

Figure 6 is concerned with spectra obtained on cooling from 110 to 60 K. At T = 80 K (figure 6(*c*)), the crystal is still in the tetragonal phase: from the splitting of the two outer lines, we measure $\Phi = 6.7°$. An abrupt alteration of the EPR lines is observed near 80 K, which points out a second phase transition ($T_{c2} \simeq 80$ K). The isotropic A line shifts towards low magnetic field values, while the splitting between the lines related to the double cubic A line decreases (figure 6(*d*)). This transition may be tentatively compared with the tetragonal to orthorhombic transition which happens near 50 K in pure $RbCaF_3$. A better understanding of this transition needs further investigation of the EPR spectrum of the Gd^{3+}–O^{2-} pair in pure $RbCaF_3$ near T = 50 K. A preliminary experiment seems to indicate the spectrum in $RbCaF_3$ to be but slightly affected by this second transition, which does not agree with the present case. However, the polydomain character of the samples makes the spectra difficult to interpret straightaway.

4.2. $Rb_{0.8}K_{0.2}CaF_3$

We investigated the temperature dependence of the A lines in the x = 0.2 mixed crystal in the same way. The modifications of the spectrum shown in figures 7 and 8 evidence two structural phase transitions in this crystal, which occur at $T_{c1} \simeq 240$ K and $T_{c2} \simeq$ 165 K. The large width of the spectral lines and the polydomain sample prevents precise results. However, owing to the splitting of the A double line, the first phase change may be due to the same mechanism as in $Rb_{0.95}K_{0.05}CaF_3$ and $RbCaF_3$. If this is true, it may be inferred that the largest value of Φ is about 5° (figure 8(*b*)). At the second transition, a shift of the low-field A line is observed as in the previous case.

4.3. *Concluding remarks*

From our results, we can draw the phase diagram shown in figure 9. The phase symmetries are extrapolated from the corresponding ones in $RbCaF_3$. The transition temperatures T_{c1} and T_{c2} are raised when x increases, while the temperature range of the intermediate

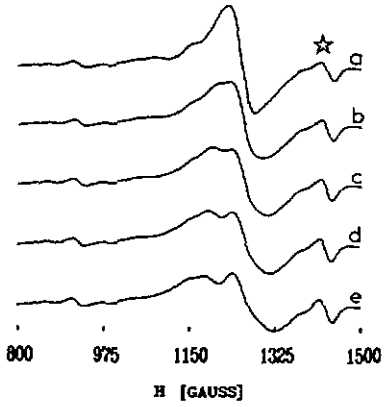

Figure 7. Temperature dependence of the A lines in $Rb_{0.8}K_{0.2}CaF_3$ about the first SPT: (*a*) $T = 240$ K, (*b*) 239 K, (*c*) 237 K, (*d*) 235 K and (*e*) 230 K. The additional line (marked by a star) is a transition that becomes allowed for $x = 0.2$ owing to the changes into the spin Hamiltonian parameters induced by the substituted K.

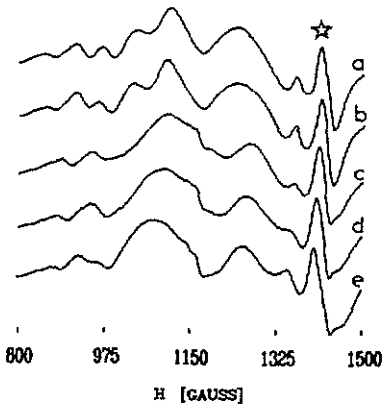

Figure 8. Temperature dependence of the A lines in $Rb_{0.8}K_{0.2}CaF_3$ about the second SPT: (*a*) $T =$ 180 K, (*b*) 170 K, (*c*) 160 K, (*d*) 130 K and (*e*) 90 K.

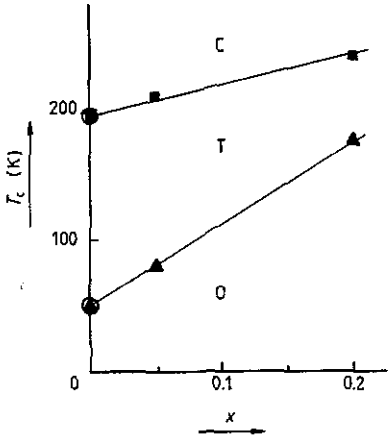

Figure 9. Phase diagram as deduced from EPR measurements in $Rb_{1-x}K_xCaF_3$ at low x ($\Delta T_c =$ 5 K).

phase shrinks. From the linear concentration dependence of T_c shown in figure 9, we obtain

$$dT_{c1}/dx \simeq 240 \text{ K} \qquad \text{and} \qquad dT_{c2}/dx \simeq 580 \text{ K}.$$

These results seem correct if we bear in mind the T_c values in $RbCaF_3$ and $KCaF_3$.

From the experiments, the two successive transitions that are observed seem to take place more abruptly in $Rb_{0.95}K_{0.05}CaF_3$ than in $Rb_{0.8}K_{0.2}CaF_3$. Thus, there is some evidence that a rounding of the discontinuities occurs gradually with increasing x.

Finally, the average rotation angle Φ of the fluorine octahedra appears to remain the order parameter of the first transition in the two compounds. The measurements of Φ

indicate that the maximum value of Φ in the tetragonal phase decreases when x increases: for $x = 0$, 0.05 and 0.2, we get $\Phi = 7.2°$, 6.7° and 5° respectively.

5. Conclusions

In this paper, we have shown the efficiency of the local Gd^{3+}–O^{2-} probe for EPR investigations of different features of the mixed fluoperovskites $Rb_{1-x}K_xCaF_3$.

A method for computing the spectra was developed, which constitutes a useful tool to obtain quantitative information on the distortion around the probe. For low values of x, we could verify the random substitution of the potassium ions at room temperature.

Cooling the samples enables us to point out two successive structural phase transitions through the temperature dependence of a particular spectrum. The transition temperatures were found to increase upon substitution of Rb with K. If the first transition is a cubic to tetragonal change, further investigations are needed in order to understand fully the mechanisms implied in the second one.

Acknowledgments

We are indebted to Professor Joël Emery for helpful discussions and G Niesseron for technical assistance in crystal growth.

References

Almairac R, Rousseau M, Gesland J Y, Nouet J and Hennion B 1977 *J. Physique* **38** 1429
Al'tschuler S A and Kozyrev B M 1974 *EPR in Compounds of Transition Elements* (New York: Wiley)
Borsa F, Benard D J, Walker W C and Baviera A 1977 *Phys. Rev.* B **15** 84
Bulou A, Nouet J, Hewatt A W and Shafer F J 1980a *Ferroelectrics* **225** 375
Bulou A, Ridou C, Rousseau M, Nouet J and Hewatt A W 1980b *J. Physique* **41** 87
Bulou A, Theveneau H, Trokiner A and Papon P 1979 *J. Physique Lett.* **40** L277
Buzaré J Y, Berlinger W and Muller K A 1985 *J. Physique Lett.* **46** L201
—— 1989 *Europhys. Lett.* **10** 739
Buzaré J Y, Fayet-Bonnel M and Fayet J C 1980 *J. Phys. C: Solid State Phys.* **13** 857
—— 1981 *J. Phys. C: Solid State Phys.* **14** 67
Buzaré J Y, Rousseau J J and Fayet J C 1977 *J. Physique Lett.* **38** L445
Buzaré J Y and Simon P 1984 *J. Phys. C: Solid State Phys.* **17** 2681
Foucher P, Buzaré J Y, Ridou C, Rousseau M and Hennion B 1990 *Ferroelectrics* **107** 325
Hidaka M, Yamashita S and Okamoto Y 1984 *Phys. Status Solidi* **81** 177
Hidaka M, Zhou Z Y and Yamashita S 1990 *Phase Transitions* **20** 83
Jouanneaux A, Leble A, Fayet J C and Fourquet J L 1989 *J. Phys.: Condens. Matter* **1** 4585
Newman D J and Urban W 1975 *Adv. Phys.* **24** 793
Ratuszna A 1984 *Phase Transitions* **4** 217
Ridou C, Rousseau M and Bouillot J 1981 *Ferroelectrics* **36** 463
Ridou C, Rousseau M and Freund A 1977 *J. Physique Lett.* **38** L359
Rousseau M, Nouet J and Almairac R 1977 *J. Physique* **38** 1423
Simon P, Rousseau J J and Buzaré J Y 1982 *J. Phys. C: Solid State Phys.* **15** 5741